2020 IEEE/RSJ International Conference on Intelligent Robots and Systems (IROS)
October 25-29, 2020, Las Vegas, NV, USA (Virtual)

Analysis, Development and Evaluation of Electro-Hydrostatic Technology for Lower Limb Prostheses Applications*

Federico Tessari[1,2], Renato Galluzzi[1], Andrea Tonoli[1], Nicola Amati[1], Matteo Laffranchi[2] and Lorenzo De Michieli[2]

Abstract— **This paper presents electro-hydrostatic actuation as a valid substitute of electro-mechanical devices for powered knee prostheses. The work covers the design of a test rig exploiting linear electro-hydrostatic actuation. Typical control laws for prosthesis actuators are discussed, implemented and validated experimentally. Particularly, this work focuses on position and admittance control syntheses enhanced with feed-forward friction compensation. Finally, the efficiency of the test rig is characterized experimentally and compared to that of classical electro-mechanical designs. It is demonstrated that the electro-hydrostatic prototype is able to fulfill its targets from a control perspective, while also having the potential to outperform electro-mechanical actuation in efficiency.**

Index Terms— **electro-hydrostatic actuator, prosthesis, knee, control, admittance, active**

I. Introduction

Robotic actuation systems have shown substantial improvements recently in terms of performance and compactness. Biorobotics, in particular, has followed this trend for the development of fully-active prosthetic systems. In this context, most of the solutions available in literature and commerce are of electro-mechanical type: they exploit a purely mechanical conversion mechanism, thus leading to complex, bulky and cost-ineffective transmission systems [1], [2].

Electro-Hydrostatic Actuation (EHA) stands as an alternative to electro-mechanical systems. It combines a linear or rotary hydraulic actuator coupled to a fixed-displacement pump by means of a two-line closed circuit. The addition of an electric machine to the input shaft of the pump yields a device with high degree of controllability. Moreover, the resulting system is intrinsically reversible, as it can work both in active and damping quadrants.

EHA systems have been proposed as actuators and/or dampers in aerospace [3], [4], automotive [5], [6] and industrial scenarios [7]. In biorobotics, EHA was initially proposed as a viable technology for robotic hands in miniature scale [8]–[10]. Kaminaga *et al.* also proposed an EHA system as a lower-limb power assistive device [11].

EHA architectures have also been proposed for ankle and knee prostheses and orthoses. Tian Yu *et al.* demonstrated that EHA provides sufficient power for an ankle prosthesis during foot push-off and lift [12]. Kaminaga *et al.* have dealt with knee [13] and ankle-knee joint systems and their control [14]. Fang *et al.* designed a EHA-based ankle prosthesis showing its high power density and its capability to smoothly interchange passive and active operations [15]. Recently, Lee *et al.* modeled and implemented a polycentric knee exoskeleton using electro-hydrostatic actuation highlighting its better efficiency and its higher power-to-weight ratio compared to electro-mechanical actuation [16].

Although several works addressed the control of prosthetic and orthotic devices [17]–[19], EHA devices have been partially addressed from a control perspective. The prototypes that appear in literature arise as a proof of concept, without giving details about the control laws that govern them. Hence, it is the aim of this paper to present a simple and reliable configuration of EHA system for a knee prosthesis device, that serves as a test rig for the implementation of different control strategies typical for prosthetic devices in the four quadrants of the force-speed plane. To this end, we first present the test rig architecture and main parameters. Then, we discuss position control, admittance control and feed-forward friction compensation. These techniques are demonstrated experimentally using the EHA test rig. Finally, the efficiency performance of the studied test rig is compared to an electro-mechanical alternative to highlight the potentiality of EHA.

II. Test rig design

To conduct this research, a test rig was designed by targeting the functionality of a powered knee prosthetic device. This system is presented in Fig. 1.

A top-down approach was followed to size this system, starting from the kinematic constraints of the application and ending on the electric machine selection.

From a biomechanical perspective, the device is characterized by angular range of motion, angular speed and torque at the level of the knee joint. We based our selection on the work by Bovi *et al.* [20], which yields useful gait cycle profiles for the knee in terms of angular trajectory, torque and power. Fig. 2 shows these trajectories in level walking condition, where the knee angular speed was computed by means of numerical derivation.

Their data is useful to demonstrate that the knee works mainly as a damper during level walking. This feature opens up the possibility of implementing power-oriented control laws to increase the autonomy of a powered joint.

*This work has been funded by INAIL/Rehab Technologies Laboratory in the Italian Institute of Technology.

[1]Department of Mechanical and Aerospace Engineering, Politecnico of Torino, Corso Duca degli Abruzzi, 24, 10129 Torino TO, Italy, federico.tessari@polito.it

[2]Rehab Technologies, Italian Institute of Technology, Via Morego, 30, 16163 Genova GE, Italy

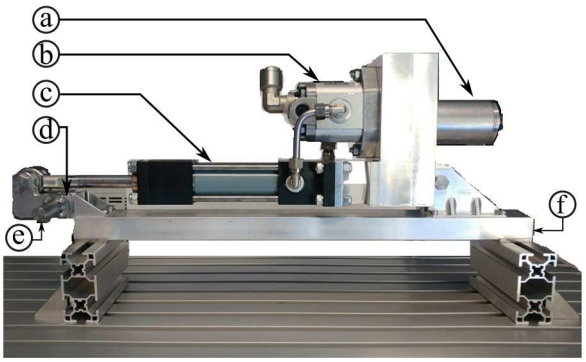

Fig. 1. EHA prototype: (a) electric motor, (b) external gear pump, (c) hydraulic cylinder, (d) knee joint, (e) thigh-connector, (f) shin/pylon.

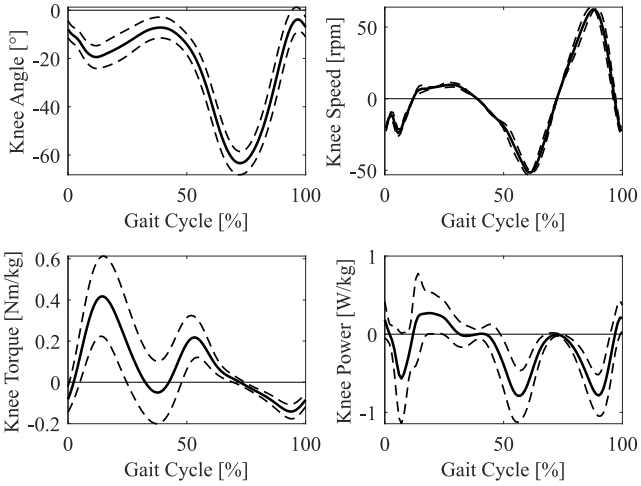

Fig. 2. Level walking knee biomechanical requirements. Solid lines represent average trends, whereas dashed ones denote variability within a standard deviation.

For the present application, the actuator sizing was based on level walking requirements to favor compactness. Power values were quantified in the ranges $-59.25 \div 20.25\,\mathrm{W}$ for a patient of 75 kg, where the positive sign implies mechanical active power delivered by the prototype. From an actuation perspective, this range is obtained by applying torque and angular speed at the knee joint within $-10.50 \div 31.50\,\mathrm{Nm}$ and $-51.53 \div 62.31\,\mathrm{rpm}$, respectively. To guarantee useful operation in a wide variety of activities, a range of motion of 110° was chosen [21].

A linear EHA solution was preferred over rotary variants, as it distributes the actuator mass along the leg main axis, unlike rotary actuators. Moreover, a linear actuation over the knee joint generates an angle-dependent transmission ratio. This non-linearity can be exploited to accommodate walking conditions. In fact, during the gait cycle, two opposite conditions are present, i.e. stance (high torque request) and swing (high speed request).

A sketch of the linear kinematics actuation can be found in Fig. 3, where θ_k represents the knee angle of rotation, h the perpendicular lever arm and c the piston stroke.

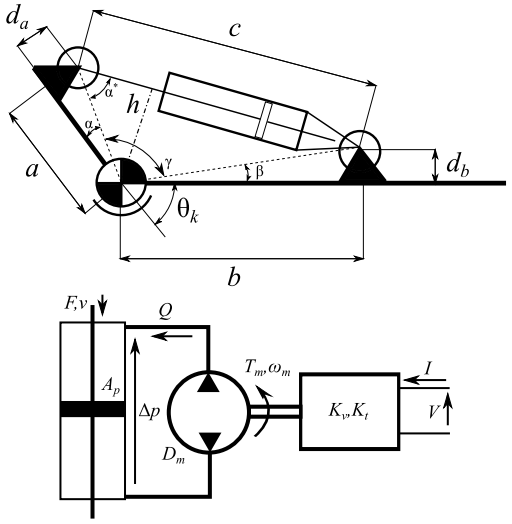

Fig. 3. Knee joint linear kinematics actuation equipped with EHA (top). EHA layout scheme (bottom).

The lever arm h relates knee quantities T_k, ω_k to linear actuation ones F, v and represents the transmission ratio between the rotary and linear system, as presented in (1).

$$h = \frac{T_k}{F} = \frac{v}{\omega_k} \tag{1}$$

The geometrical quantities describing the kinematics were set to: $a = 30\,\mathrm{mm}$, $b = 340\,\mathrm{mm}$ and $d_a = d_b = 20\,\mathrm{mm}$. These values were selected to guarantee the required ROM without exceeding anthropometric dimensions of lower limbs [22], [23].

The selected kinematic layout led to an EHA with a useful stroke $x = 60\,\mathrm{mm}$, maximum required force $F_{max} = 1.2\,\mathrm{kN}$ and speed $\mathrm{v_{max}} = 0.2\,\mathrm{m/s}$.

To guarantee F_{max} while accounting for mechanical losses, a safety factor $S = 2$ was applied to this value. The hydraulic piston was designed and custom-built as a double-rod end device to guarantee symmetry in both directions. The cross section was selected to limit the actuator pressure drop to $\Delta p_{max} = 60\,\mathrm{bar}$:

$$A_p = \frac{SF_{max}}{\Delta p_{max}} \cong 3.78\,\mathrm{cm}^2 \tag{2}$$

The hydraulic cylinder ports are directly connected to those of hydraulic pump. Assuming ideal efficiency, the pump displacement was selected to bound its angular speed at $\omega_{max} = 6\,\mathrm{krpm}$. This allows a safe, cavitation-free operation, while also preserving the mechanical components of the electric machine.

$$D_m = \frac{A_p v_{max}}{\omega_{max}} \cong 0.75\,\mathrm{cm}^3/\mathrm{rev} \tag{3}$$

Thus, a Bucher APR05/0.75 external-gear reversible pump was selected for the task. The hydraulic cylinder and pump

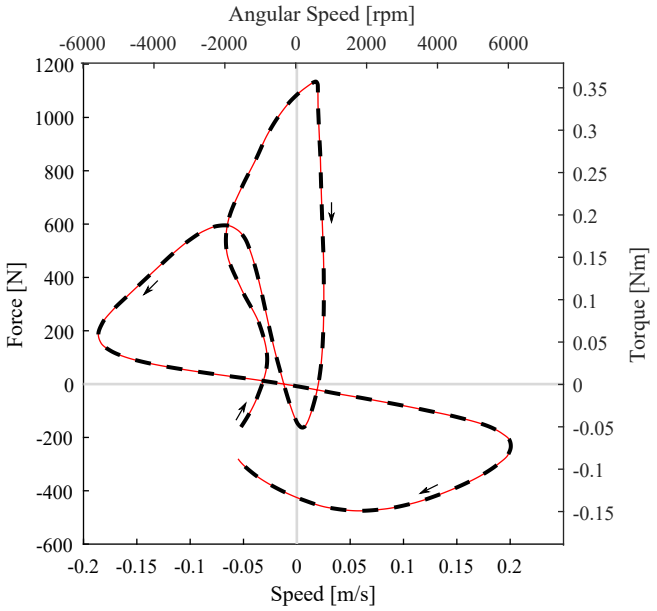

Fig. 4. Level walking knee biomechanical requirements expressed in the hydraulic actuator force-speed plane (dashed) and the electric motor torque-angular speed plane (solid). Unitary efficiency is considered. The progression over the gait cycle is represented by the arrows.

choices lead to a transmission defined by the ratio

$$\tau = \frac{D_m}{A_p} = 1.98\,\text{mm/rev} \tag{4}$$

which, in ideal conditions, yields a direct relationship between the output force/speed and the input torque/angular speed at the level of the electric motor:

$$\tau = \frac{T_{max}}{SF_{max}} = \frac{\omega_{max}}{v_{max}} \tag{5}$$

From (5), the maximum torque for the electric machine is defined as

$$T_{max} = \tau SF_{max} = 0.76\,\text{Nm} \tag{6}$$

For this purpose, a Maxon EC-i 40 brushless DC motor was selected. Although the motor is able to yield 0.21 Nm in continuous operation, transient bursts up to 2.86 Nm are available for ten seconds, if required.

Figure 4 resumes the four quadrants biomechanical requirements of knee during level walking in two different planes: the hydraulic cylinder force-speed one and the electric motor torque-angular speed one. The chart assumes unitary efficiency and confirms how the knee during level walking works mainly as brake-damper, since its force-speed trajectory lays in the II and IV quadrants.

III. Control

The developed EHA was then used to implement a set of different control strategies to demonstrate the validity of this type of actuation for a powered knee prosthetic device.

The actuation was equipped with an analog encoder and a torque transducer at the knee joint level to measure both the knee angular position and its torque. Moreover, the electric motor was equipped with digital Hall sensors to implement a six-step current control. The developed strategies were implemented on a Texas Instruments TMS28335 real-time digital signal processing unit. Figure 5 illustrates the experimental setup.

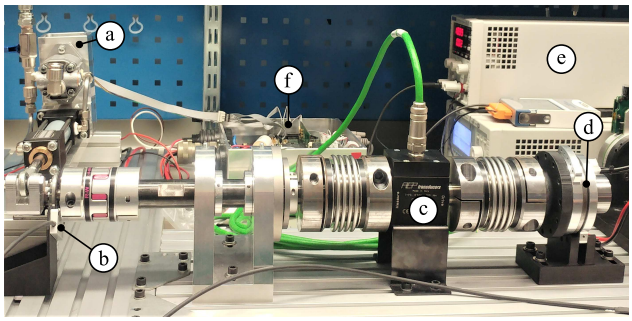

Fig. 5. Experimental test rig: (a) EHA prototype, (b) knee joint absolute encoder, (c) knee torque transducer, (d) load drive, (e) power supply, (f) control and power stage.

We present two main strategies that are knee position control and admittance control. These strategies are inspired by Lawson *et al.* previous works that analyzed gait in powered lower limb prosthetic devices [18], [19]. They showed that impedance-admittance-based controllers can enhance gait coordination and natural walking, while decreasing the number of control parameters.

Moreover, an additional subsection will describe a feedforward control law that aims at minimizing the effects of friction.

A. Knee Position Control

Position control, or position tracking, consists in the capability of a given plant/system to follow a specific trajectory. In the case of prosthetic and orthotic devices, these trajectories are typically extracted from biomechanical data.

Position control is required for a correct implementation of the admittance controller. Moreover, it is analyzed to demonstrate the capability of the actuation to reproduce the knee joint trajectories in different gait conditions. These are fed to the position control loop reference $\theta_{k_{ref}}$ as presented in Figure 6.

The position control loop implements a parallel PI controller. Proportional and integral gains were tuned to guarantee most favorable reference tracking for the tested profiles. The position control loop execution frequency was set to $f_s = 2\,\text{kHz}$, i.e. one decade smaller than the current loop.

B. Admittance Control

Admittance and impedance controls are used in either service or industrial robotics, particularly when there is the need of interacting with the environment. For example, an admittance controller establishes a desired dynamic behavior (stiffness, damping, inertia) to the prosthetic device. This type of control is mandatory for appropriate interaction of the prosthesis with the user and the environment. The controller compares the desired trajectory θ_{k_0} with the one computed from the dynamic model. This yields the angular position

reference $\theta_{k_{ref}}$ that feeds the position control. In turn, the position loop sets the current reference i_{ref} for the motor control algorithm (see Figure 6).

$$\theta_{k_{ref}} = \theta_{k_0} + \theta_{dyn} \tag{7}$$

$$\theta_{dyn} = \frac{T_{k_m}}{J_{k_{des}} s^2 + \beta_{k_{des}} s + k_{k_{des}}} \tag{8}$$

In this specific application, the EHA was configured to simulate a visco-elastic system. Hence, we assumed $J_{k_{des}} = 0$ and analyzed the behavior of the actuator while varying the desired stiffness $k_{k_{des}}$ and viscous damping $\beta_{k_{des}}$.

1) Spring-Damper Behavior: A visco-elastic system can be considered as a parallel combination of a spring and damper. In such system, the required desired dynamics are expressed by Eq. (9).

$$\theta_{dyn} = \frac{T_{k_m}}{\beta_{k_{des}} s + k_{k_{des}}} \tag{9}$$

A discrete version of this transfer function was obtained by means of Tustin's approximation, which sets

$$s = 2 f_s \frac{1 - z^{-1}}{1 + z^{-1}} \tag{10}$$

Combining Eqs. 9 and 10 yields

$$\theta_{dyn} = \frac{T_{k_m}(1 + z^{-1})}{(-\beta_{k_{des}}(2f_s) + k_{k_{des}}) z^{-1} + (\beta_{k_{des}}(2f_s) + k_{k_{des}})} \tag{11}$$

$$\theta_{dyn}(k) = \frac{T_{k_m}(k) + T_{k_m(k-1)}}{\beta_{k_{des}}(2f_s) + k_{k_{des}}} - \theta_{dyn}(k-1) \frac{-\beta_{k_{des}}(2f_s) + k_{k_{des}}}{\beta_{k_{des}}(2f_s) + k_{k_{des}}} \tag{12}$$

C. Feed-Forward Friction Compensation

Feed-forward control strategies are often implemented to compensate the presence of disturbances in a control loop system. Specifically, in the developed test rig EHA, the hydraulic cylinder presented standard gasket seals with high stiction and stick-slip effect. Gasket seals are also present on the shaft of the gear pump to avoid oil leakages, thus further worsening friction nonlinearity.

These features motivate the introduction of a feed-forward compensation term i_c to the reference signal that feeds the electric machine current loop. This term attempts to compensate the disturbance d_f introduced by the aforementioned effects. The control scheme block diagram is then presented in Fig. 6.

In literature several works investigated friction modeling and its feed-forward compensation [24], [25]. In this work, a simple strategy governed by Eq. (13) was implemented

$$i_c = K_f \cdot \text{sign}\left(\dot{\theta}_k\right) \tag{13}$$

Equation (13) relates the compensation current i_c to the sign of the angular speed of the knee $\dot{\theta}_k$ by means of the coefficient K_f. This coefficient needs to be properly tuned in order to mitigate the friction as much as possible while also avoiding the excessive injection of current.

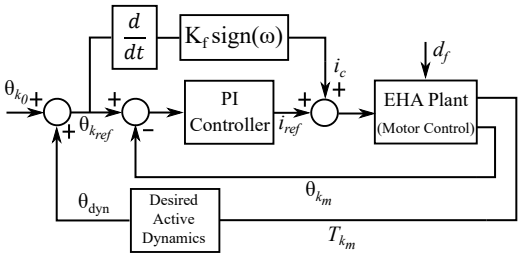

Fig. 6. High-level control strategy including: admittance control (outer loop), position control (inner loop) and feed-forward friction compensation.

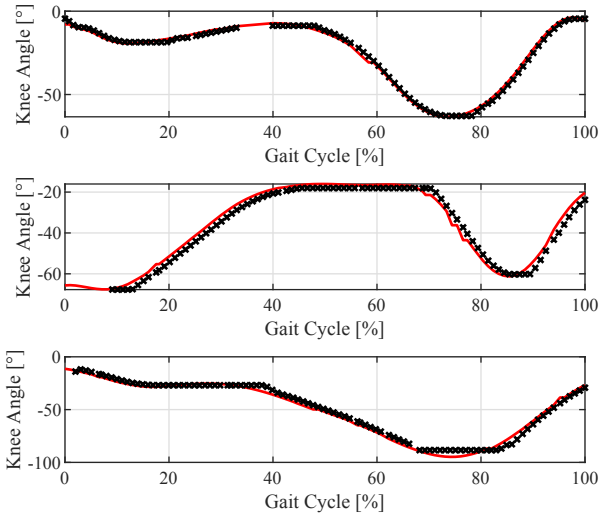

Fig. 7. Experimental position control with different knee trajectories: level walking (top), step ascending (middle), step descending (bottom). Continuous lines represent the reference signals while crosses the measured values.

IV. EXPERIMENTAL RESULTS

A. Knee Position Control

The position control loop tests evaluated the capability of the EHA to reproduce the following gait conditions: level walking (LW), step ascending (SA) and step descending (SD). The trajectories were extracted from [20] and they constitute typical gait profiles. The obtained results are presented in Figure 7.

The system is able to reproduce all the given trajectories with acceptable tracking error. Specifically the root-mean-squared errors between the reference trajectory and the obtained ones are, respectively: $RMSE_{LW} = \pm 1.5°$, $RMSE_{SA} = \pm 2.8°$, $RMSE_{SD} = \pm 3.4°$.

B. Visco-Elastic Admittance Control

The admittance control experiments aim at validating the EHA capability of reproducing visco-elastic behavior. For this purpose, two different set of tests were performed. A first attempt demonstrates the ability of the system to reproduce different elastic behaviors. The viscous damping was kept constant and very low ($\beta_{k_{des}} = 6 \cdot 10^{-4}$ Nms/rad)

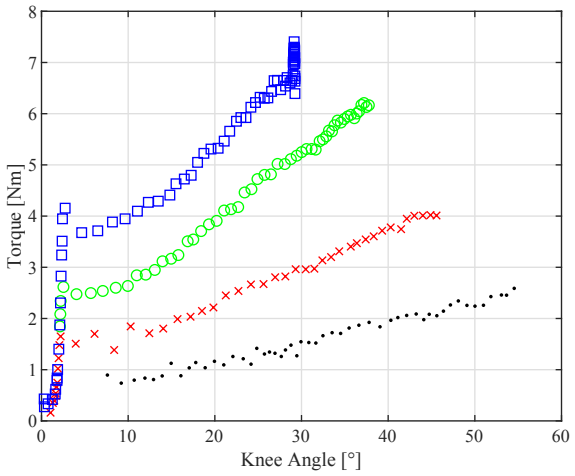

Fig. 8. Knee torque-angle behavior varying stiffness: 2.29 Nm/rad (dot), 4.58 Nm/rad (cross), 9.17 Nm/rad (circle), 13.75 Nm/rad (square). Viscous damping was kept constant: $\beta_{k_{des}} = 6 \cdot 10^{-4}$ Nms/rad.

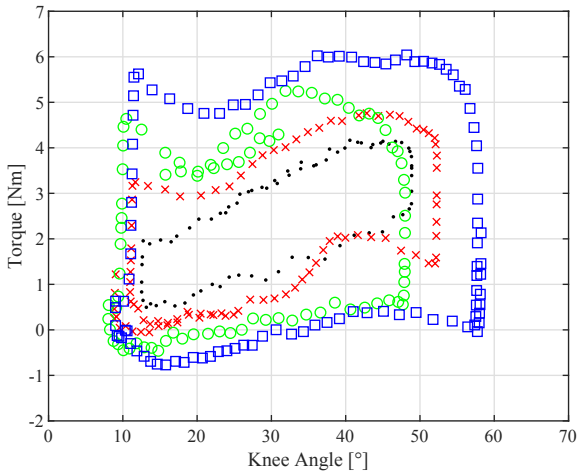

Fig. 9. Knee torque-angle behavior varying viscous damping: 0.06 Nms/rad (dot), 0.6 Nms/rad (cross), 1.2 Nms/rad (circle), 1.7 Nms/rad (square). Stiffness was kept constant: $k_{k_{des}} = 4.58$ Nm/rad.

in order to enhance the stiffness characteristic. Then, four different values of $k_{k_{des}}$ were applied. In a second set, tests were performed by imposing four different damping values $\beta_{k_{des}}$, while keeping a relatively low stiffness value $k_{k_{des}} = 4.58$ Nm/rad.

According to the control strategy presented in Fig. 6, a nominal position $\theta_{k_0} = 0°$ was kept. Figures 8 and 9 present the obtained results.

In particular, Fig. 8 shows that the system can reproduce the desired stiffness target in all cases. However, although a feed-forward compensation was implemented to mitigate stiction and stick-slip effects, the presence of this phenomenon is still noticeable by the offset of the torque-angle characteristics with respect to the vertical axis.

Figure 9 highlights the viscous behavior; it shows that an increase in the damping value produces a larger hysteresis behavior in the torque-angle plot. Also in this case, the feed-forward friction compensation could not completely mitigate the actuator stick-slip effect, which can be observed by the increasing square shape of the torque-angle characteristic.

These results are in agreement with the expectations since the developed EHA is sub-optimal, not only in terms of integration, but also regarding performances (see Section III-C). More favorable results are expected with an optimized and integrated custom electro-hydrostatic actuator.

C. Efficiency Mapping

A test campaign was performed to measure the overall transmission efficiency of the system, i.e. the ratio between output mechanical power P_{out} and input electrical power P_{in}:

$$\eta = \frac{P_{out}}{P_{in}} = \frac{T_k \cdot \omega_k}{V_{bus} \cdot I_{bus}} \tag{14}$$

A position control loop has been implemented, while, by means of an electric motor coupled to a harmonic drive, a dynamic load was imposed to the EHA.

The experimental and simulated efficiency maps are presented in Fig. 10. The prototype presents maximum and average efficiencies of 31.2% (at $T_k = 15$ Nm, $\omega_k = 30$ rpm) and 18.8%, respectively, within the tested torque-speed range.

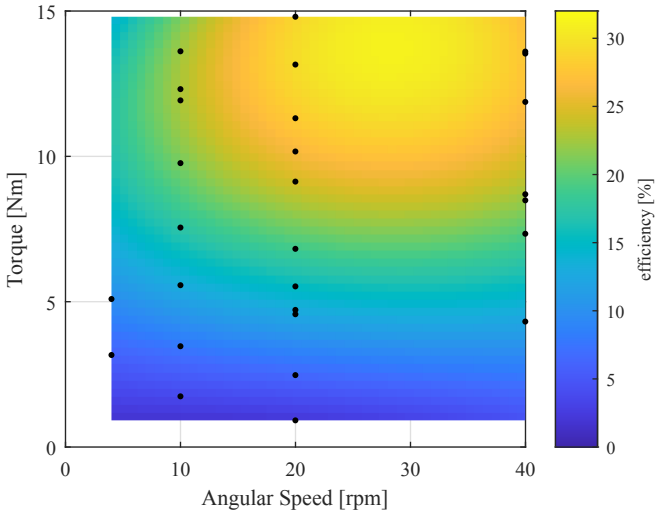

Fig. 10. EHA transmission experimental efficiency. The tested torque-angular speed points at the load (dot) were numerically interpolated to produce a color map.

The efficiency of an electro-mechanical actuation has been computed to provide a direct comparison with the developed EHA. This alternative system would combine the same brushless motor with a harmonic drive targeting the same ratio τ_{avg}. This system would lead to an efficiency (based on datasheet information) of $\eta_{EM} \approx 27\%$ in the same working condition.

As previously indicated, the rig used in these tests is not optimized both in terms of performance and size. However, its peak efficiency is comparable but slightly higher than state-of-the-art electro-mechanical systems designed with classical approaches. Moreover, this does not represent a definitive result, but a useful evaluation that highlights the high potential of EHA solutions.

V. CONCLUSIONS

This paper presented the analysis, design and experimental evaluation of a test rig electro-hydrostatic actuator (EHA) for a powered knee prosthetic device. The design input requirements came from biomechanical and anthropometric data available in literature. Following this initial requirements analysis phase, this work proposes an intuitive actuator components' selection: hydraulic cylinder, pump and electric motor. The test rig was assembled using off-the-shelf components. Then, the work focused on control strategies for active lower limb devices and their implementation. In particular, the authors presented the design of a visco-elastic admittance controller. Three different test sets have been performed. The first one demonstrated the capability of the developed EHA to precisely reproduce biomechanical knee trajectories in three conditions: level walking, step ascending and step descending. The second one analyzed the proposed admittance control strategy by imposing a visco-elastic dynamics to the EHA. Different stiffness and damping values have been imposed and experimentally validated. Finally, a last test campaign focused in evaluating the actuator performance in terms of actuation efficiency.

The prototype was assembled with non-optimized and non-integrated off-the-shelf components that introduced friction-related issues. Despite these drawbacks, the obtained results represent a promising starting point for powered lower limb prostheses. In fact, the developed EHA demonstrated to be a more suitable solution compared to classical electromechanical actuation thanks to its competitive efficiency performance and good controllability.

Further developments will involve the design of a fully custom integrated and optimized EHA to overcome the presented issues and to move from test rig analysis to on-filed validation.

REFERENCES

[1] D. S. Pieringer, M. Grimmer, M. F. Russold, and R. Riener, "Review of the actuators of active knee prostheses and their target design outputs for activities of daily living," in *Proc. International Conference on Rehabilitation Robotics (ICORR)*, QEII Centre, London, UK, July 2017, pp. 1246–1253.

[2] Össur, *Power Knee: Instruction for use / patient*, 2012.

[3] R. Galluzzi, A. Tonoli, and N. Amati, "Modeling, Control, and Validation of Electrohydrostatic Shock Absorbers," *Journal of Vibration and Acoustics*, vol. 137, no. 1, p. 011012, 2015.

[4] R. Navarro, "Performance of an electro-hydrostatic actuatore on the f-18 systems research aircraft," NASA, Dryden Flight Research Center, Tech. Rep., 1997.

[5] C. O'Shea, Y. Xia, and S. Lowry, "Analysis and optimization of an electrohydraulic power pack for use in a fully-active vehicle suspension through the use of computational fluid dynamics," in *Proceedings of the ASME/BATH 2013 Symposium on Fluid Power & Motion Control, FPMC2013*, 2013, v001T01A002.

[6] R. Galluzzi, Y. Xu, N. Amati, and A. Tonoli, "Optimized design and characterization of motor-pump unit for energy-regenerative shock absorbers," *Applied Energy*, vol. 210, no. 1, pp. 16–27, 2018.

[7] D. Belloli, F. Previdi, S. M. Savaresi, A. Cologni, and M. Zappella, "Modeling and identification of an electro-hydrostatic actuator," in *Proc. IFAC Symposium on Mechatronic Systems*, Cambridge, Massachusetts, USA, sep 2010, pp. 620–625.

[8] H. Kaminaga, T. Yamamoto, J. Ono, and Y. Nakamura, "Backdrivable miniature hydrostatic transmission for actuation of anthropomorphic robot hands," in *Proc. IEEE-RAS International Conference on Humanoid Robots*, Pittsburgh, PA, USA, nov 2007, pp. 36–41.

[9] H. Kaminaga, T. Amari, Y. Takayama, J. Ono, Y. Shimoyama, and Y. Nakamura, "Backdrivability analysis of electro-hydrostatic actuator and series dissipative actuation model," in *Proc. IEEE International Conference on Robotics and Automation*, Anchorage, Alaska, USA, may 2010, pp. 4204–4211.

[10] A. Kargov, T. Werner, C. Pylatiuk, and S. Schulz, "Development of a miniaturised hydraulic actuation system for artificial hands," *Sensors and Actuators A Physical*, vol. 141, no. 2, pp. 548–557, 2008.

[11] H. Kaminaga, T. Amari, Y. Niwa, and Y. Nakamura, "Electro-hydrostatic actuators with series dissipative property and their application to power assist devices," in *Proc. IEEE International Conference on Biomedical Robotics and Biomechatronics*, Tokyo, Japan, sep 2010, pp. 76–81.

[12] T. Yu, A. Plummer, P. Iravani, J. Bhatti, S. Zahedi, and D. Moser, "Testing and electrohydrostatic powered ankle prosthesis with transtibial and transfemoral amputees," in *Proc. IFAC Symposium on Mechatronic Systems*, Loughborough University, Leicestershire, UK, sep 2016, pp. 185–191.

[13] H. Kaminaga, J. Ono, Y. Nakashima, and Y. Nakamura, "Development of backdrivable hydraulic joint mechanism for knee joint of humanoid robots," in *Proc. IEEE International Conference on Robotics and Automation*, Kobe, Japan, may 2009, pp. 1577–1582.

[14] H. Kaminaga, S. Otsuki, and Y. Nakamura, "Design of an ankle-knee joint system of a humanoid robot with a linear electro-hydrostatic actuator driven parallel ankle mechanism and redundant biarticular actuators," in *Proc. IEEE International Conference on Humanoid Robots*, Atlanta, Georgia, USA, oct 2013, pp. 384–389.

[15] J. Fang, X. Wang, R. Li, S. Wang, and W. Wang, "Active ankle prosthesis powered by electrohydrostatic actuation technology: Design and implementation," in *CSAA/IET International Conference on Aircraft Utility System (AUS 2018)*. Guiyang, China: IET, June 2018, pp. 1170–1175.

[16] T. Lee, D. Lee, B. Song, and Y. Su-Baek, "Design and control of a polycentric knee exoskeleton using an electro-hydrualic actuator," *Sensors*, vol. 20, no. 1, pp. 1–20, 2020.

[17] G. Aguirre-Ollinger, J. E. Colgate, M. A. Peshkin, and A. Goswami, "Active-impedance control of a lower-limb assistive exoskeleton," in *IEEEE 10th International Conference on Rehabilitation Robotics*, Noordwijk, The Netherlands, June 2007, pp. 188–195.

[18] B. E. Lawson and M. Goldfarb, "Impedance & admittance-based coordination control for robotic lower limb," *Mechanical Engineering Magazine*, vol. 136, no. 09, pp. 12–17, 2014.

[19] B. E. Lawson, J. E. Mitchell, D. Truex, A. Shultz, E. Ledoux, and M. Goldfarb, "A robotic leg prosthesis: Design, control and implementation," *IEEE Robotics & Automation Magazine*, vol. 21, no. 4, pp. 70–81, 2014.

[20] G. Bovi, M. Rabuffetti, P. Mazzoleni, and M. Ferrarin, "A multiple-task gait analysis approach: Kinematic, kinetic and emg reference data for healthy young and adult subjects," *Gait & Posture*, vol. 33, no. 1, pp. 6–13, 2011.

[21] Y. S. Anouchi, M. McShane, F. K. Jr., J. Elting, and J. Stiehl, "Range of motion in total knee replacement," *Clinical Orthopaedics and Related Research*, vol. 331, no. 1, pp. 87–92, 1996.

[22] D. A. Winter, *Biomechanics and Motor Control of Human Movement: Fourth Edition*. Hoboken, New Jersey, USA: John Wiley & Sons, Inc., 2009.

[23] H. D. Associates and A. R. Tilley, *The Measure of Man and Woman: Human Factors in Design*. Hoboken, New Jersey, USA: John Wiley & Sons, 2001.

[24] G. Borghesan and C. Melchiorri, "Model and modeless friction compensation: Application to a defective haptic interface," in *Proc. 6th International Conference on Haptics: Perception, Devices and Scenarios*, Madrid, Spain, jun 2008, pp. 94–103.

[25] Y. Liu, J. Li, Z. Zhang, X. Hu, and W. Zhang, "Experimental comparison of five friction models on the same test-bed of the micro stick-slip motion system," *Mechanical Sciences*, vol. 6, no. 1, pp. 15–28, 2015.